LOW FREQUENCY WAKE DYNAMICS OF CANTILEVERED CIRCULAR CYLINDERS AT AN ASPECT RATIO OF 4

Chris Morton
Department of Mechanical & Manufacturing Eng.
University of Calgary
2500 University Dr. NW, Calgary, Alberta, Canada
chris.morton@ucalgary.ca

Mohammad Saeedi
Department of Aerospace Engineering
Amirkabir University of Technology
Tehran, Iran
mohammad.saeedi@aut.ac.ir

Maryam Shahroodi, Matthew Kindree, Robert J. Martinuzzi
Department of Mechanical & Manufacturing Eng.
University of Calgary
2500 University Dr. NW, Calgary, Alberta, Canada
mshahroo@ucalgary.ca , mgkindre@ucalgary.ca, rmartinu@ucalgary.ca

ABSTRACT

Near-wake characteristics of a low aspect ratio ($h/d = 4$) cantilevered circular cylinder protruding a thin laminar boundary layer have been investigated both experimentally ($Re = 10,400$) and numerically ($Re = 300$). Despite the substantial differences in the investigated Re, the unsteady wake topology exhibits similar instability mechanisms: (i) a Kármán-like vortex shedding instability, and (ii) a low-frequency instability which manifests as a coupling between the flow over the free end and the base flow near the cylinder-wall junction. Attention is drawn to the low-frequency instability, which comprises a significant portion of the kinetic energy content in the wake, and has not been reported in previous experimental or numerical investigations. It appears to be characteristic of intermediate aspect ratio cantilevered circular geometries.

INTRODUCTION

The flow across cantilevered bluff bodies is ubiquitous in the natural environment and in industrial applications, *e.g.*: wind loadings on trees, buildings, cross-flow heat exchangers and chimney stacks. Hence, it is not surprising that such geometries have been the subject of a multitude of experimental and numerical studies over the last century (*e.g.*, Fox & Apelt (1993), Rodi (1997), Okamoto & Yagita (1973), Martinuzzi & Havel (2004), Rostamy *et al.* (2012)). Previous experimental studies on cantilevered bluff bodies have shown that the flow development and related structural loading characteristics strongly depend on the oncoming boundary layer characteristics, the body aspect ratio and the Reynolds number Re of the flow based on the characteristic length scale of the body (e.g., Okamoto & Yagita (1973) and others). It is widely accepted that above a critical aspect ratio, the oscillatory dynamics due to a vortex shedding instability dominate the wake development.

For Reynolds numbers relevant to turbulent vortex shedding conditions, the dominant vortical structures exhibit significant temporal modulations in their strength (amplitude) which are linked to a low-frequency drift in the base flow (Bourgeois *et al.*, 2013). The base flow modulation is resolvable with Proper Orthogonal Decomposition (POD) analysis and is consistent with mean-field theory (Stuart, 1958): an energetic exchange exists between the modes associated with vortex shedding and the low-frequency shift mode (Noack *et al.*, 2003). At low Re, this energetic exchange occurs at the onset of the vortex shedding instability (Noack *et al.*, 2003), until the system reaches a dynamically stable state with a constant shedding amplitude. For higher Re turbulent flows, Bourgeois *et al.* (2013) showed that the vortex shedding is continuously perturbed from its limit-cycle oscillation and this process is modelled well with mean-field theory. Presently, it remains unclear if a low-frequency shift mode persists for all turbulent bluff body wakes exhibiting quasi-periodic vortex shedding.

The focus of the present study is to investigate laminar and turbulent vortex shedding from a cantilevered circular cylinder of aspect ratio 4. The goal is to identify the dominant energetic structures in the wake, and provide insight into low frequency phenomena occurring under both laminar and turbulent shedding conditions.

METHODOLOGY

The flow development over a low aspect ratio ($h/d = 4$) cantilevered circular cylinder is investigated for $Re = 300$ and $10,400$. For the test case $Re = 300$, results are from numerical simulation, while experiments have been conducted for $Re = 10,400$ in a wind tunnel facility. For brevity, the test cases will be referred to by their Reynolds number.

Numerical Methodology

Simulations were carried out using the open-source code package of Field Operation and Manipulation (OpenFoam) on a parallel platform with 64 processors. The computational domain consists of a structured O-type mesh around the cylinder and an H-type in the remainder of the domain which has been refined following the procedure of McClure *et al.* (2015). A Dirichlet boundary condition us-

ing a laminar boundary layer profile is imposed at the inlet. The laminar boundary layer thickness at the cylinders location is $\delta/d = 2$. A Newmann boundary condition is imposed at the domain outlet, a free-slip (zero wall shear stress) boundary condition is imposed at the upper surface and side boundaries, and a no-slip boundary condition is set on the ground plane and cylinder surfaces. Time-resolved numerical data were acquired for a duration of over 150 shedding cycles. A vortex shedding frequency f_{sh} was identified from velocity measurements yielding a Strouhal number of $St = f_{sh}d/U_\infty \approx 0.144$. Post processing of flow-field data was carried out in a three-dimensional wake region as well as in a planar rectangular wake region approximately matching that of the PIV experiment.

Experimental Methodology

Experiments were conducted in an open-test-section wind tunnel. A circular cylinder with $h/d = 4$ (diameter of $d = 12.7$ mm) was mounted on a flat plate $16.8d$ from the leading edge. The laminar boundary layer thickness was approximately $\delta/d = 0.20$ at the obstacle location. The freestream speed was $U_\infty \approx 14.3$ m/s giving $Re = U_\infty d/\nu = 10,400$. A vortex shedding frequency f_{sh} was identified from both velocity and surface pressure measurements yielding a Strouhal number of $St = f_{sh}d/U_\infty \approx 0.145$, similar to that obtained for the simulation.

Three-component velocity fields $\mathbf{u} = (u,v,w)$ in xy-planes were measured using a *LaVision Flow Master* stereoscopic particle image velocimetry (SPIV) system. Olive oil particles of 1 µm mean diameter were generated by a Laskin nozzle nebulizer and illuminated by a 1.5 mm thick laser sheet from a Photonics Nd:YLF laser. Two Photron SA4 CMOS cameras with 1024 by 1024 pixel resolution, separated by 60°, captured SPIV image pairs at 1600 Hz. This sampling frequency provided approximately 10 samples per shedding cycle and 1360 cycles in total over five trials. *LaVision's DaVis* 8.3 software was used to process the SPIV images with an interrogation window size of 16×16 pixels with 50 % overlap. The vector field spanned $1.2 \leq x/d \leq 6.5$, $-2.7 \leq y/d \leq 2.7$ with a uniform vector spacing of $0.04d$.

RESULTS

In this study, the flow over a cantilevered cylinder was found to comprise of two dominant wake features as detected from analysis of surface pressure and wake velocity fluctuations: (i) a vortex shedding instability centred on f_{SH}, and (ii) a low frequency activity centred on approximately $f_{SH}/4$. Direct evidence of these flow features is provided in Figs. 1-3. Figure 1 shows the autocorrelation of pressure fluctuations on the cylinder surface with the lag-time axis non-dimensioned with f_{SH}. At both $Re = 300$ and $10,400$, a periodic signature is centred on approximately $f_{SH}/4$ as confirmed in the corresponding spectra of p in Fig. 2. Spectra of the w fluctuations reveal a composite signal containing both f_{SH} and $f_{SH}/4$ behaviour (Fig. 3). To the authors' knowledge, the low-frequency behaviour has not been reported before for cantilevered cylinders in cross-flow. Thus follow-up experiments were done yielding the following observations: the low-frequency phenomenon is not observed (i) in experiments where the boundary layer is tripped (*i.e.*, turbulent); (ii) on cantilevered cylinders with a higher aspect ratio, and (iii) on square cross-section cantilevered bodies. This suggests the unique behavior is a fun-

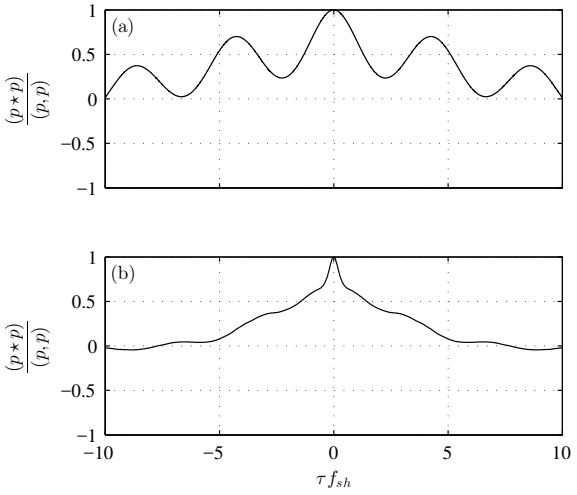

Figure 1. Normalized autocorrelation of pressure fluctuations on the cantilevered cylinder surface at $(x/d, y/d, z/d)$ = (0.5,0,2) for: (a) $Re = 300$, (b) $Re = 10,400$.

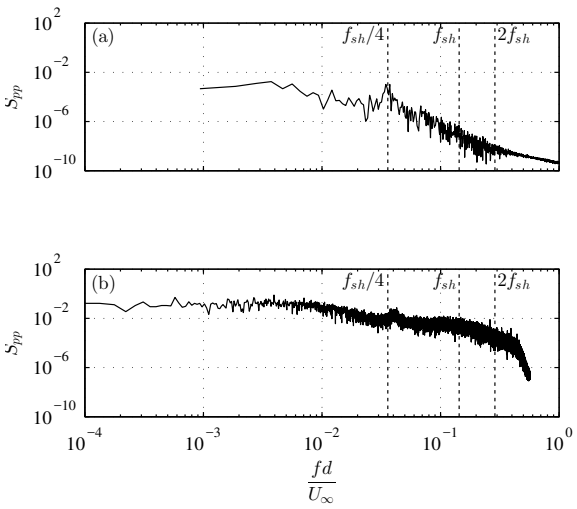

Figure 2. Spectral analysis of pressure fluctuations on the surface of a cantilevered cylinder at $(x/d, y/d, z/d)$ = (0.5,0,2) for: (a) $Re = 300$, (b) $Re = 10,400$.

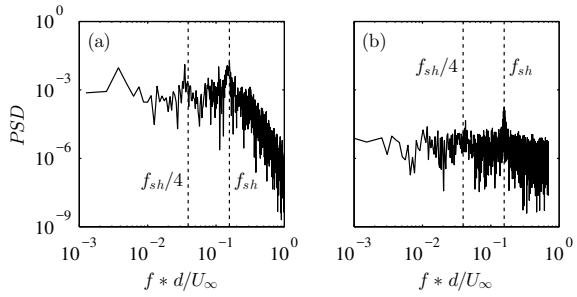

Figure 3. Spectral analysis of w fluctuations in the wake of a cantilevered cylinder at $(x/d, y/d, z/d)$ = (4,1,2) for: (a) $Re = 300$, (b) $Re = 6,800$.

damental, Reynolds number independent process. Hence, it is of value to be diagnostically studied through the three-dimensional, time-resolved laminar flow simulation results obtained in the present work.

To confirm the the low-frequency phenomenon at $\sim f_{SH}/4$ at $Re = 300$ and $Re = 10,400$ corresponds to the same fundamental process, planar velocity field data obtained at the cylinder mid-span were analysed using POD. Note that the flow field is divided into symmetric and anti-symmetric components following Holmes *et al.* (2012). Figure 4 shows the normalized modal energy distribution of the first ten symmetric and anti-symmetric POD modes for the experimental and numerical data sets. The seven most energetic POD modes (two from the anti-symmetric and five from the symmetric field) represent 60% and 40% of the total energy fluctuation energy, $\mathbf{K}$. Here, $\mathbf{K} = \int\int_{\Omega} k \mathrm{d}x\mathrm{d}y = \sum_{i=1}^{N} \lambda_i$, where Ω is the observation domain and N is the total number of modes. The difference in relative energy content between $Re = 300$ and $10,400$ is attributed to the existence of turbulent energy content at smaller scales for $Re = 10,400$ distributed in the higher-order modes (Fig. 4). Analysis of the seven most energetic POD modes in the base and near-wake region indicate that the underlying flow phenomenology and large-scale dynamics are strikingly similar for the simulated laminar case at $Re = 300$ and the experimental turbulent wake at $Re = 10,400$. Six of these modes contain a strong periodic content, forming mode pairs. The spatial modal functions for each of the three velocity components and the normalized power spectral density function, *psdf*, are shown for three modes for $Re = 300$ and $Re = 10,400$ in Fig. 5 and 6, respectively. The most energetic mode pair appears in the asymmetric field and is associated with the first harmonic, f_{SH}. In the symmetric field, the least energetic mode pair are associated the second harmonic, $2f_{SH}$. These modes resemble those described by Bourgeois *et al.* (2013) and are closely associated with shedding of vortices.

The three most energetic modes in the symmetric field accounts for approximately 10-15% of $\mathbf{K}$. From the *psdf* for both *Re*, the spectral energy is concentrated at much lower frequencies than for the previous modes. For two of these modes, a distinct spectral peak at $\sim St/4$ indicates a significant periodic contribution (*e.g.,* Fig. 6). In contrast to the fundamental harmonic mode associated with periodic vortex shedding, the spatial mode for the u field is symmetric, while that for the v field is antisymmetric and the u-fluctuations contribute considerably more than the other two components to $\mathbf{K}$ (Fig. 5e-h and 6e-h). This mode also shows most of the energy fluctuation at low frequencies, but the energy contribution around $f_{SH}/4$ is significantly weaker (*e.g.,* Fig. 5). The motion described by these three modes is similar for both *Re* and accounts for a slow-varying base flow and an additional periodic instability distinct from that of the vortex shedding mechanism.

Analysis of 3D Numerical Simulation Data

To elucidate the nature of the $f_{SH}/4$ phenomenon and the associated slow-varying base flow, detailed analysis is carried out on the 3D numerical simulation data. Figure 7 depicts important features of the mean 3D velocity field in the wake at $Re = 300$: (1) an isosurface of $u = 0$ in Fig. 7a illustrates the 3D recirculation zone extending nearly 5D downstream of the cylinder; (2) planar slices of mean u illustrate the wake development and its recovery from $x/D = 0$ to $x/D = 10$ (Figs. 7a-b); (3) surface streamline patterns in Fig. 7c indicate the presence of a quadrupole structure downstream of the recirculation zone; (4) surface streamline patterns in Fig. 7d highlight the downwash over the free end as well as tip and base mean field structures within the recirculation zone. The mean field topology is in agreement with that shown by Sumner *et al.* (2004) for a cantilevered cylinder of similar aspect ratio.

Figure 8 shows instantaneous visualizations of the vortical structures shed into the wake at arbitrary shedding phases. Analysis of video sequences of the vortex shedding revealed that the primary spanwise vortices deform substantially as they are shed into the wake region and form hairpin-like structures. In particular, the spanwise vorticity at formation is reoriented through vortex tilting and stretching, and is speculated to be the primary cause for the quadropole structure identified in the mean field, in agreement with Bourgeois *et al.* (2011). In order to investigate the influence of the $f_{SH}/4$ modes on the wake dynamics, the role and relationship between the POD modes was further investigated. In a first instance, a low-order reconstruction of the flow field was formulated using the mean field and the three most-energetic modes of the symmetric field. Analysis of these results over several time intervals suggests that the combined influence of these modes is two-fold. First, these modes describe a slow-varying drift of the base flow, *i.e.* a low-frequency variation of the streamwise extent of the recirculation region. This behaviour is similar to that reported by Noack *et al.* (2003) and Bourgeois *et al.* (2013). Second, these modes also describe a spanwise (motion normal to the wall) oscillation of the base flow at period of approximately $4/f_{SH}$. This behaviour is consistent with the observations made from the modal distributions described above: (i) this vertical motion is symmetric about y=0 and contributes little to v fluctuations and is thus very different from the asymmetric motion described by the fundamental harmonic (*i.e.,* the vortex shedding); and (ii) these modes are not associated directly with the formation of vortical structures.

The three low-frequency modes may thus be considered to be related to instabilities arising near the cantilevered body. The question thus arises whether an interaction between these modes and the higher frequency modes can be described and whether the interaction is related to mean-field theory. To this end, the behaviour of the modal coefficients is more closely considered. Figure 9a-c show excerpts of time traces for three temporal coefficients: the fundamental harmonic pair a_1^a, a_2^a from the asymmetric field and the slow-varying mode a_Δ for which the spectrum shows only a weak energetic contribution around $f_{SH}/4$. The modulation of the harmonic temporal coefficients is related to a_Δ similarly to that described by Noack *et al.* (2003) and Bourgeois *et al.* (2013). The amplitude of the fundamental harmonic modes is largest for large positive values of a_Δ and significantly smaller as a_Δ approaches a (negative) minimum. Moreover, the time-averaged amplitude corresponds to values for which $a_\Delta \approx 0$.

The phase portrait of the coefficients a_2^a *vs* a_1^a is shown in Fig. 9d. In the figure, the radius of the red circle represents the time-average amplitude of the harmonic fluctuation. The data suggests that the amplitude of the harmonic fluctuation varies about a limit cycle described by the red circle. The non-random nature of this variation becomes clearer when viewing the 3D phase portrait a_Δ *vs* a_1^a, a_2^a as shown in Fig. 9e. The resulting paraboloid is direct evidence that the amplitude of the harmonic fluctuation is related to the slow-varying motion described through a_Δ.

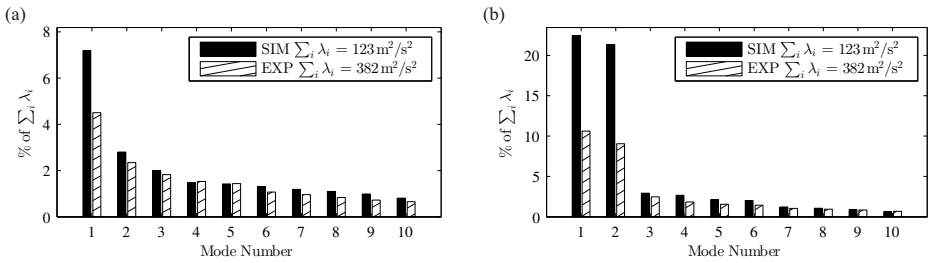

Figure 4. Modal energy distribution obtained from the POD of velocity measurements: (a) Symmetric fluctuating field, (b) Antisymmetric fluctuating field. $TKE = \sum_i \lambda_i$

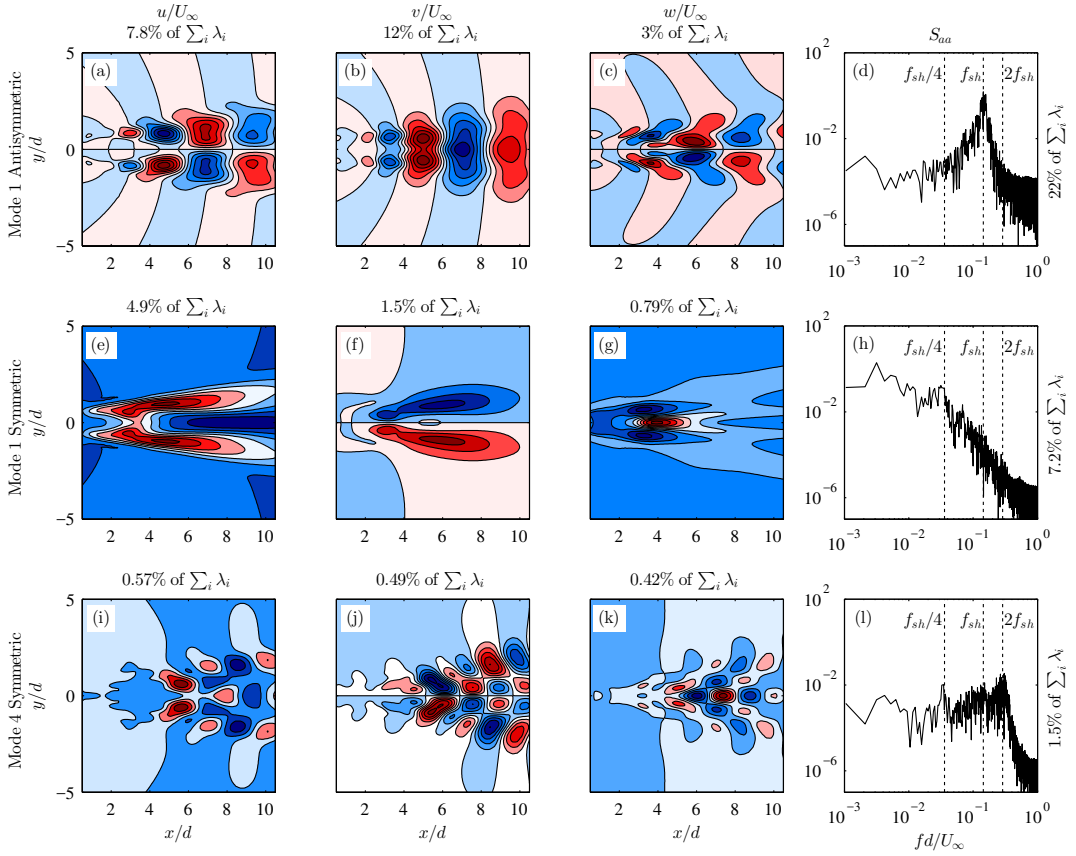

Figure 5. Spatial modal functions for each of the three velocity components and the normalized power spectral density function, *psdf*, for $Re = 300$.

From a dynamical systems perspective, the paraboloid in Fig. 9e describes the departures of the quasi-steady vortex shedding from its limit cycle oscillation. This observation is consistent with mean-field theory, whereby the transient response to a perturbation of the harmonic oscillation due to vortex shedding follows a trajectory towards the limit-cycle along the paraboloid relating the three modes considered. For higher Reynolds numbers, the action of turbulence is sufficient to perturb the vortex shedding process to naturally exhibit the response resulting in a paraboloid (Bourgeois *et al.*, 2013). For lower (laminar) Reynolds numbers, the transient behaviour must be forced through some additional instability. Interestingly, as seen in Fig. 9c for intervals $120 < t < 240$ or $420 < t < 470$, periodic fluctuations of a_Δ around $f_{SH}/4$ are expressed when the amplitude of the temporal coefficient is low and the amplitude of the vortex shedding is small. In other words, the $f_{SH}/4$ phenomenon is manifested in a_Δ when the vortex shedding has become weakened by perturbations in the field.

CONCLUSIONS

The flow development over a low aspect ratio (h/d = 4) cantilevered circular cylinder was investigated for $Re = 300$ and $10,400$. It is shown that the wake dynamics consists of two dominant instability mechanisms: (i) a vortex shedding instability of characteristic frequency f_{sh}, and (ii) a low-frequency instability of characteristic frequency approximately $1/4 \cdot f_{sh}$. The low-frequency instability is identified as the most energetic periodic POD mode in the symmetric field, and is accompanied by a low frequency drift in the base flow. The low-frequency phenomenon is shown to

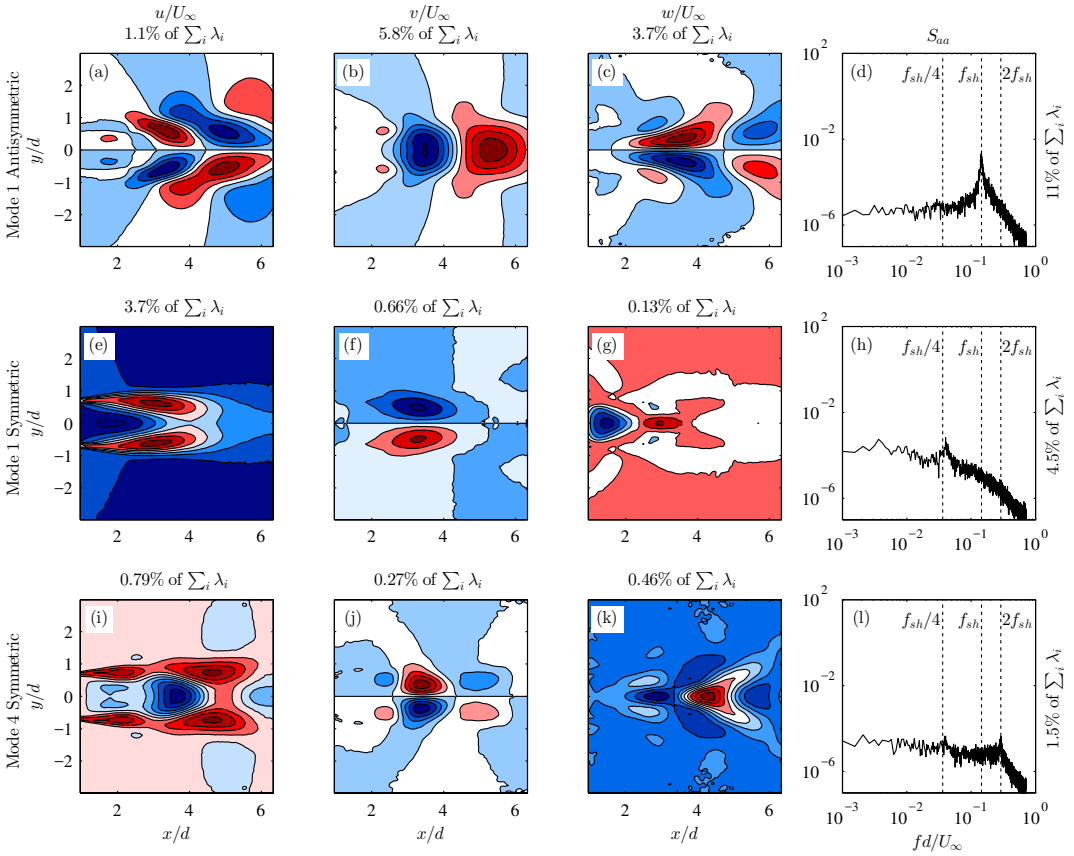

Figure 6. Spatial modal functions for each of the three velocity components and the normalized power spectral density function, *psdf*, for $Re = 10,400$.

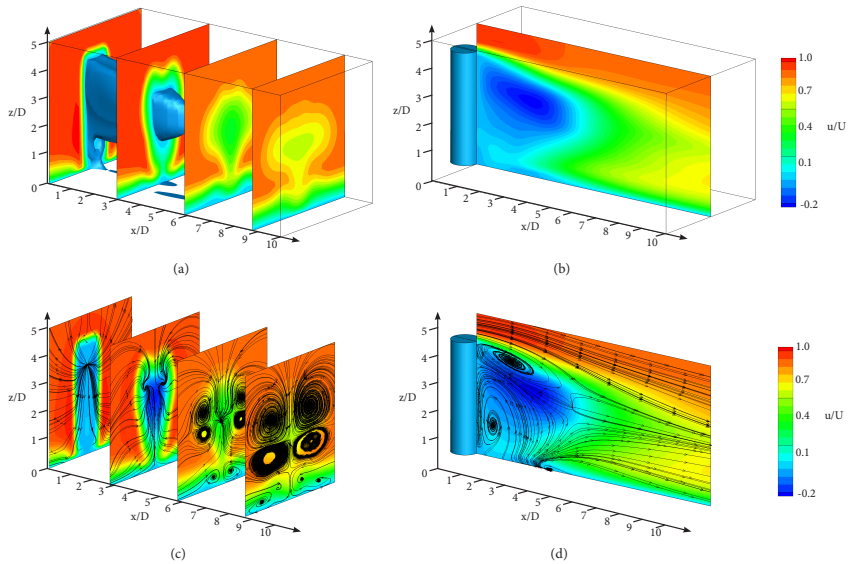

Figure 7. Three-dimensional mean velocity field characteristics and topological streamline flow features for $Re = 300$.

be a flapping instability which modulates the wake region. Moreover, the instability becomes amplified when the primary vortex shedding is weak.

REFERENCES

Bourgeois, J. A., Noack, B. R. & Martinuzzi, R. J. 2013 Generalized phase average with applications to sensor-based flow estimation of the wall-mounted square cylinder wake. *J. Fluid Mech.* **736**, 316–350.

Bourgeois, J. A., Sattari, P. & Martinuzzi, R. J. 2011 Al-

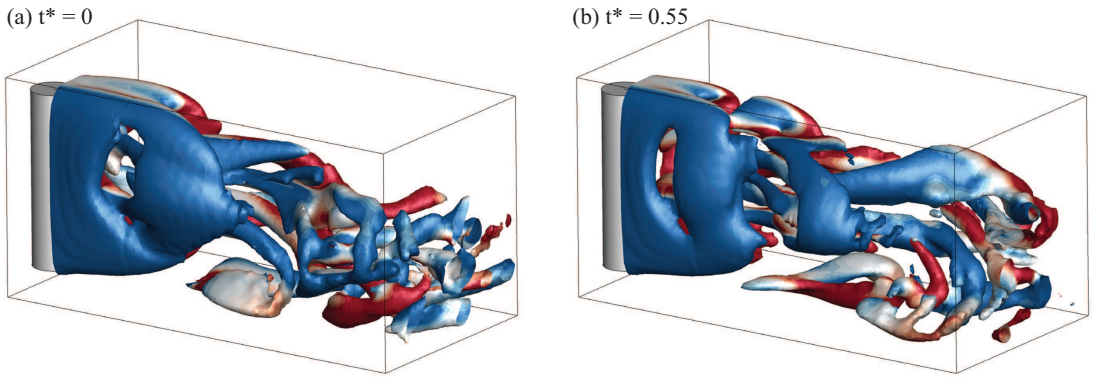

Figure 8. Instantaneous vortical structures in the wake of a cantilevered cylinder for $Re = 300$. t^* is the number of vortex shedding periods.

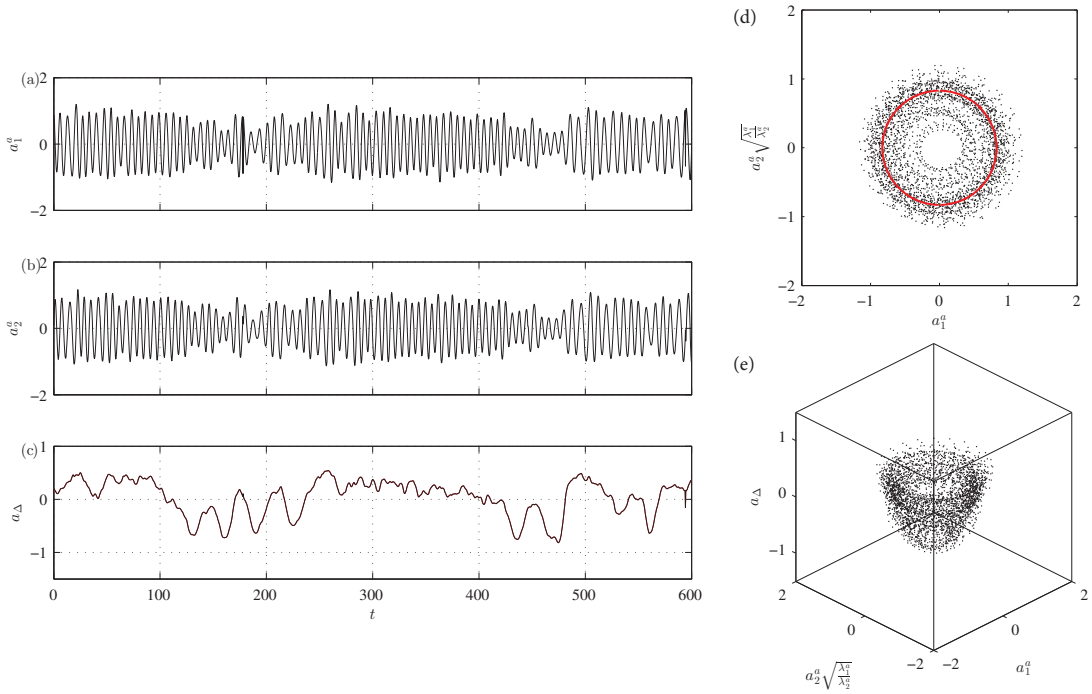

Figure 9. Temporal coefficients and their correlations obtained from three-dimensional POD applied to a cantilevered cylinder wake at $Re = 300$.

ternating half-loop shedding in the turbulent wake of a finite surface-mounted square cylinder with a thin boundary layer. *Phys. Fluids* **23**, 095101, 1–15.

Fox, T. A. & Apelt, C. J. 1993 Fluid induced loading of cantilevered circular cylinders in a low–turbulence uniform flow. part 3: Fluctuating loads with aspect ratios 4 to 25. *J. Fluids Struct.* **7**, 375–386.

Holmes, P., Lumley, J.L, Berkooz, G. & Rowley, G.W. 2012 *Turbulence, coherent structures, dynamical systems and symmetry*, 2nd edn. Cambridge university press.

Martinuzzi, R. J. & Havel, B. 2004 Vortex shedding from two surface-mounted cubes in tandem. *Int. J. Heat Fluid Flow* **25**, 364–372.

McClure, J, Morton, C & Yarusevych, S 2015 Flow development and structural loading on dual step cylinders in laminar shedding regime. *Phys. Fluids* **27** (6), 063602.

Noack, Bernd R, Afanasiev, Konstantin, Morzynski, Marek, Tadmor, Gilead & Thiele, Frank 2003 A hierarchy of low-dimensional models for the transient and post-transient cylinder wake. *Journal of Fluid Mechanics* **497**, 335–363.

Okamoto, T. & Yagita, M. 1973 The experimental investigation on the flow past a circular cylinder of finite length placed normal to the plane surface in a uniform stream. *Bull. Japan Soc. Mech. Eng.* **16**, 805–814.

Rodi, W. 1997 Comparison of LES and RANS calculations of the flow around bluff bodies. *J. Wind Eng. Ind. Aero.* **69**, 55–75.

Rostamy, N., Sumner, D., Bergstrom, D. J. & Bugg, J. D. 2012 Local flow field of a surface-mounted finite circular cylinder. *J. Fluids Struct.* **34**, 105–122.

Stuart, J. T. 1958 On the non-linear mechanics of hydrodynamic stability. *Journal of Fluid Mechanics* **4**, 1–21.

Sumner, D., Heseltine, J. L. & Dansereau, O. J. P. 2004 Wake structure of a finite circular cylinder of small aspect ratio. *Exper. Fluids* **37**, 720–730.